

Exploring the association between coronary vascular anatomical features and future myocardial infarction through statistical shape modelling

Original

Exploring the association between coronary vascular anatomical features and future myocardial infarction through statistical shape modelling / Griffo, Bianca; Rizzini, Maurizio Lodi; Candreva, Alessandro; Collet, Carlos; Mizukami, Takuya; Chiastra, Claudio; Gallo, Diego; Morbiducci, Umberto; Aldieri, Alessandra. - In: JOURNAL OF BIOMECHANICS. - ISSN 0021-9290. - ELETTRONICO. - 189:(2025), pp. 1-11. [10.1016/j.jbiomech.2025.112829]

Availability:

This version is available at: 11583/3001212 since: 2025-06-23T08:10:55Z

Publisher:

Elsevier

Published

DOI:10.1016/j.jbiomech.2025.112829

Terms of use:


This article is made available under terms and conditions as specified in the corresponding bibliographic description in the repository

Publisher copyright

(Article begins on next page)



Exploring the association between coronary vascular anatomical features and future myocardial infarction through statistical shape modelling

Bianca Griffo^{a,b}, Maurizio Lodi Rizzini^{a,b}, Alessandro Candreva^{a,c}, Carlos Collet^d, Takuya Mizukami^{d,e}, Claudio Chiastra^{a,b}, Diego Gallo^{a,b}, Umberto Morbiducci^{a,b}, Alessandra Aldieri^{a,b,*} 

^a Department of Mechanical and Aerospace Engineering, Politecnico di Torino, Turin, Italy

^b PoliToBIOMed Lab, Politecnico di Torino, Turin, Italy

^c Department of Cardiology, Zurich University Hospital, Zurich, Switzerland

^d Cardiovascular Center Aalst, OLV-Clinic, Aalst, Belgium

^e Department of Clinical Pharmacology, Showa University, Tokyo, Japan

ARTICLE INFO

Keywords:

Myocardial infarction
Statistical shape model
Linear discriminant analysis
Vascular geometry

ABSTRACT

Considering the intricate interplay among coronary anatomy and hemodynamics in coronary artery disease (CAD), anatomy-based descriptors have been employed as surrogates of local aberrant hemodynamics and, ultimately, as clinical markers for diagnostic and predictive purposes. However, anatomical descriptors have demonstrated unsatisfactory accuracy, making their further investigation cogent in CAD applications. Therefore, this study investigates the presence of unexplored pathological shape features of left anterior descending (LAD) coronary arteries associated with myocardial infarction (MI) at 5 years using statistical shape modelling. A statistical shape modelling framework combining principal component analysis (PCA) and linear discriminant analysis (LDA), where PCA outputs served as inputs to LDA, was applied to: (i) a cohort of 69 patient-specific LAD geometries, including both future culprit (FCL) and controls, *i.e.*, non-culprit lesions (NCL) of MI reconstructed from 3D quantitative coronary angiography; (ii) the same cohort after artificially removing the main lesion from each LAD model, aiming to isolate the contribution of the atherosclerotic burden beyond the main lesion severity, quantifiable using %AS. Using LDA, the hyperplane with significant discriminant capacity ($p < 0.0001$) between NCL and FCL was identified for both cohorts. The combination of the statistical shape modelling-based representation accounting for the atherosclerotic burden exclusive of the main lesion severity with %AS, accounting explicitly for the main lesion severity, exhibited notable discrimination capacity for future MI. This study supports the hypothesis that the overall atherosclerotic burden may predispose to future MI and highlights the potential of a statistical shape modelling-based approach for integration into current imaging-driven clinical decision-making.

1. Introduction

Atherosclerosis in coronary arteries is a complex inflammatory condition that can lead to several clinical complications. Myocardial infarction (MI) represents the most serious adverse event and it commonly results from the onset and progression of atherosclerotic lesions, eventually leading to the occlusion of a coronary vessel (Bentzon et al., 2014). Accordingly, the early identification of atherosclerotic lesions prone to cause MI has assumed prominent clinical relevance.

The entity of the pressure gradient across an atherosclerotic lesion is currently considered a clinical indicator of the risk of future adverse clinical events (De Bruyne et al., 2012; Munhoz et al., 2024). The estimation of translesional pressure gradients to assess coronary lesion severity is typically quantified indirectly in terms of fractional flow reserve (FFR) (Gurav et al., 2024; Pijls et al., 1996), either invasively by positioning pressure wires inside the vessels (Pijls et al., 1996) or with computational techniques (Candreva et al., 2022a; Haley et al., 2021). Yet, evidence has been provided that translesional pressure gradients

* Corresponding author at: PoliToBIOMed Lab, Department of Mechanical and Aerospace Engineering, Politecnico di Torino, Corso Duca degli Abruzzi, 24, 10129 Turin, Italy.

E-mail address: alessandra.aldieri@polito.it (A. Aldieri).

<https://doi.org/10.1016/j.jbiomech.2025.112829>

Accepted 19 June 2025

Available online 19 June 2025

0021-9290/© 2025 The Authors. Published by Elsevier Ltd. This is an open access article under the CC BY license (<http://creativecommons.org/licenses/by/4.0/>).

per se might not be sufficient to discriminate lesions culprit for future MI (Koo et al., 2024; Lee et al., 2019). Among possible hallmarks, the biomechanical stimuli acting at the blood-endothelium interface (i.e., the wall shear stress, WSS, and derived quantities) have been suggested to play a role in coronary artery disease (CAD) onset/progression (De Nisco et al., 2024; Hoogendoorn et al., 2020; Samady et al., 2020; Stone et al., 2018), and emerged as independent predictors of future MI (Candreva et al., 2022b; Kumar et al., 2018; Thondapu et al., 2021; Tufaro et al., 2021). However, calculating WSS is not clinically straightforward, as it relies on computational hemodynamics simulations, which are computationally intensive (Candreva et al., 2022a; Gijzen et al., 2019) and inherently subject to idealizations (Steinman and Migliavacca, 2018).

In parallel, the relationship existing between vascular anatomy and local hemodynamics (where the former shapes fluid structures) has emerged over the past few decades. The observed co-localization of anatomy-induced flow disturbances, such as flow separation and recirculation, with regions prone to coronary plaque growth has paved the way for adopting coronary anatomical attributes as surrogates of local aberrant hemodynamics (Asakura and Karino, 1990; Candreva et al., 2024; Friedman et al., 1983; Morbiducci et al., 2016; Wentzel et al., 2012). Thus, based upon the well-established principle of causality – linking the cause (anatomy) to the effect (flow disturbances and pressure losses) and ultimately to the consequence (CAD progression and MI) – anatomy-based decision making has become widely adopted by cardiologists in clinical practice.

Among the available clinical imaging technologies, visual assessment of angiographic diameter stenosis or quantitative coronary angiography (QCA) have been largely adopted because of their availability and reduced costs (Collet et al., 2024). QCA enables the assessment of specific anatomical attributes of diseased coronary arteries as lesion severity, commonly quantified in terms of percentage area stenosis (%AS, which reflects the percentage reduction in the cross-sectional area of the artery compared to its reference segment (Suzuki et al., 2020)). The use of %AS in clinical decision-making is largely adopted, particularly for percutaneous coronary intervention or MI risk assessment (Candreva et al., 2024, 2022b; Reiber et al., 1993; Suzuki et al., 2020; Uren et al., 1994). However, the capability of the anatomy-based quantities made available by the clinical imaging to discriminate future MI is still unsatisfactory (Candreva et al., 2024; Fischer et al., 2002; Stone et al., 2011), making it pivotal to further investigate coronary anatomical attributes affecting lesions/vessels propensity to future MI. In parallel, accumulating evidence is showing that adverse future coronary events are related not just to the main coronary artery luminal lesions, but rather to the overall atherosclerotic burden throughout the vessel, being it flow-limiting or not, and several studies have indeed disclosed a strong association between atherosclerotic disease burden and risk for adverse coronary events (Arbab-Zadeh and Fuster, 2015; Stone et al., 2023; Vergallo et al., 2025). In this regard, statistical shape models (SSMs), which are able to capture subtle anatomical variations across populations, may reveal differences in atherosclerotic burden and help identify vessels at risk of future MI. SSMs have already been used for unravelling associations between anatomy and functional or pathological mechanisms (Aldieri et al., 2024; Bruse et al., 2016; Cosentino et al., 2020; Cutugno et al., 2021; Liu et al., 2024; Mansi et al., 2011; Rodero et al., 2021; Romero et al., 2024; Sophocleous et al., 2022; Swanson et al., 2024; Williams et al., 2022), and have proven to be effective in identifying peculiar attributes of cardiovascular regions (Bruse et al., 2016; Mansi et al., 2011).

The overarching hypothesis of this study is that anatomical attributes of diseased coronary arteries, beyond those currently used in QCA-based clinical practice, may help discriminate the occurrence of MI at 5 years. To test this hypothesis, statistical shape modelling was applied to 3D left anterior descending coronary artery (LAD) geometries reconstructed from angiographic images of retrospectively analyzed patients (Candreva et al., 2022b), aiming to assess whether additional

anatomical attributes may contribute to identify vessels site of future MI. Technically, to investigate the relative contributions of the main lesion and the overall LAD anatomy to the risk of future MI, two distinct SSM-based analyses were carried out on the same LAD cohort: (1) the first one considering the LAD population as reconstructed from angiographic images (LAD₀), and (2) the second one considering the same LAD population with the main lesion removed from each 3D vessel geometry (LAD_{NL}).

While LAD₀ cohort reflected the overall atherosclerotic burden of the vessel (Arbab-Zadeh and Fuster, 2015; Vergallo et al., 2025), by removing the most severe lesion in each vessel to create the LAD_{NL} cohort, we purged the contribution of %AS to the atherosclerotic burden, thus retaining the widespread atherosclerotic narrowing throughout the vessel with the exclusion of the main lesion severity (quantified by %AS). The contribution of the atherosclerotic burden beyond the main lesion severity, inherently difficult to quantify, was thus isolated and considered in the LAD_{NL} cohort. Furthermore, its role was examined in comparison to %AS, which provides quantitative information only about the single most severe lesion of the vessel, but does not account for its location along the vessel or the presence of other lesions in the same vessel.

2. Materials and methods

2.1. Study population

A total of 69 patients who underwent coronary angiography for acute MI between January 2008 and December 2019 were considered for this work. Patients were part of a larger dataset (Candreva et al., 2022b) collected within a previous study conducted by three different medical centers (OLV clinic, Aalst, Belgium; University Hospital of Lausanne CHUV; Fribourg Cantonal Hospital, Switzerland), and were selected according to the following inclusion criteria: (i) MI occurrence, (ii) a coronary angiography performed between 1 month and 5 years before the event, (iii) a mild lesion ($\leq 50\%$ visually identifiable diameter reduction) culprit for future MI (future culprit lesion, FCL) and (iv) at least one other non-culprit for MI lesion (non-culprit lesion, NCL) in one of the other two major epicardial coronary arteries (Candreva et al., 2022b). Data obtained from the most recent angiography were employed for this analysis, considering only the left anterior descending coronary artery (LAD) for each patient. A total of 69 subject-specific LADs including 36 FCL and 33 NCL vessels were analyzed in this study. The median time between baseline angiography and MI was equal to 24.6 (IQR: 9.5–39.9) months (FCL: 22.4, IQR: 6.9–35.1; NCL: 29.2, IQR: 13.3–43.6). No statistical differences were found between FCL and NCL groups ($p = 0.17$).

The study protocol conforms to the ethical guidelines of the 1975 Declaration of Helsinki and has been approved by the Institutions' ethics committees. Written informed consent was obtained from each patient included in the study.

2.2. 3D anatomical reconstruction and characterization

The overall workflow followed in this study is presented in Fig. 1. Three-dimensional QCA (3D-QCA) reconstructions of the LAD arteries were generated from two orthogonal angiographic projections at least 30° apart (CAAS Workstation WSS software, Pie Medical Imaging, Maastricht, the Netherlands), as extensively reported elsewhere (Candreva et al., 2022b; Lodi Rizzini et al., 2024). The reconstructed LAD 3D geometries were used for both anatomical characterization and SSM construction. On each 3D reconstructed LAD geometry, the lesion segment (LS) was identified as the portion of the vessel containing the minimum lumen area (MLA) section. This segment was automatically bounded proximally and distally by the points where the 3D-QCA area function line intersected with the interpolated reference line, as clarified in the example in Fig. 2 (Candreva et al., 2022b; Lodi Rizzini et al.,

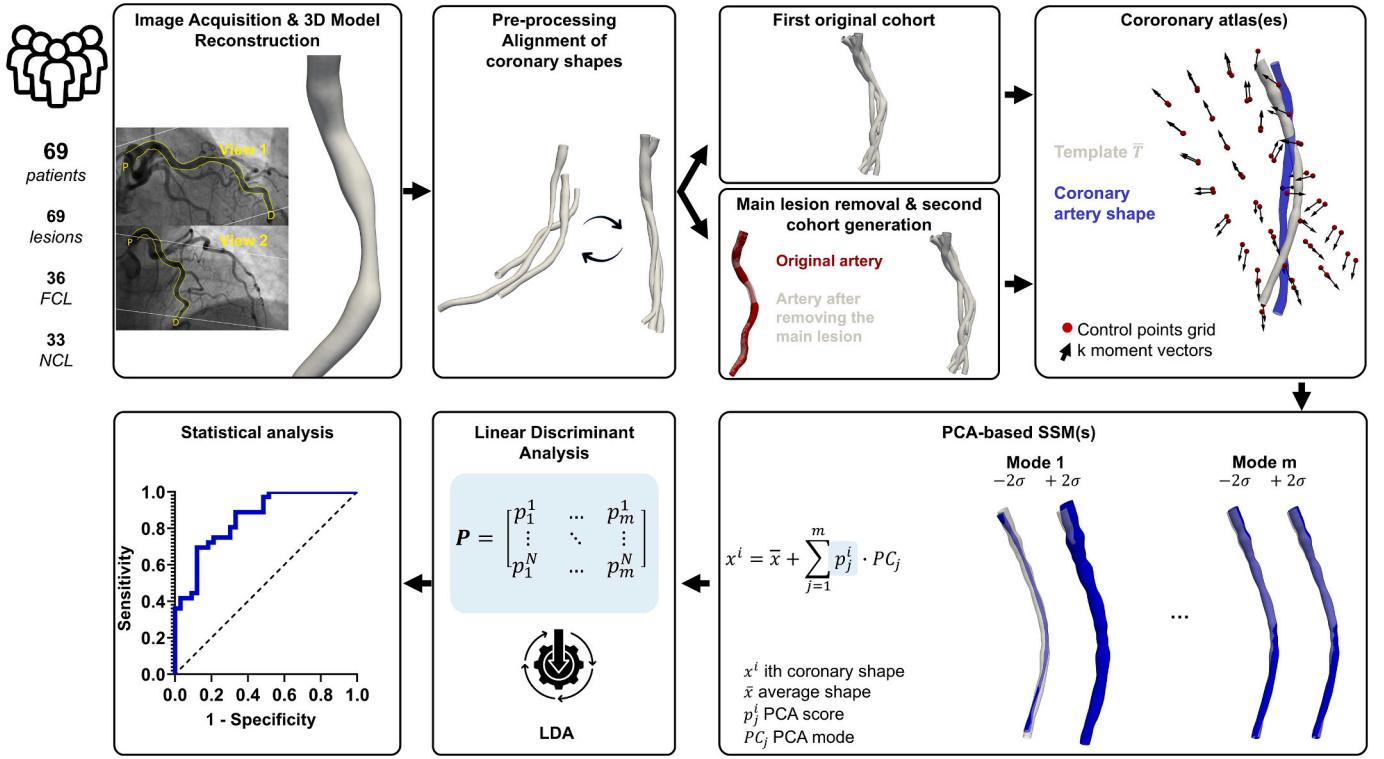


Fig. 1. Workflow adopted for the study. The LAD of 69 patients (36 FCL and 33 NCL) was considered for this study. The 3D coronary artery models were reconstructed from 3D-QCA and subsequently re-aligned and scaled during a pre-processing phase. From this, two different cohorts were obtained: (i) the original cohort, and (ii) a second cohort after removing the main lesion from each coronary artery model. Two distinct coronary atlases were built through Deformetrica, which, for each cohort, generates a template (in grey) representing the mean anatomical shape, and vessel-specific moment vectors centered at a common grid of control points (in red), morphing the template to each coronary shape (in blue). PCA was applied to the moment vectors of each cohort to build two distinct SSMs, thus retrieving the main shape modes in each case. LDA was applied on the matrices of PCA scores P to find the linear combination of PCA modes maximizing the separation between FCL and NCL. Finally, a leave-one-out cross-validation was carried out and a statistical analysis was performed to link anatomical features and future MI. (For interpretation of the references to colour in this figure legend, the reader is referred to the web version of this article.)

2024). The %AS value at the MLA, quantifying the anatomical severity of the lesion, was computed according to the clinical practice as:

$$\%AS = \frac{S_{MLA}^{ref} - S_{MLA}}{S_{MLA}^{ref}} \cdot 100 \quad (1)$$

where S_{MLA}^{ref} is the value of the surface area of the interpolated reference line located at the curvilinear coordinate of the MLA, and S_{MLA} is the value of the MLA cross-sectional surface area of the coronary artery (Candrea et al., 2022b; Lodi Rizzini et al., 2024).

The centerlines of the reconstructed LAD geometries were computed within the Vascular Modeling Toolkit (<https://www.vmtk.org>) (Antiga et al., 2008). Centerline-based attributes of coronary vessels were evaluated in terms of curvature, tortuosity, and torsion. Details on the computation of the centerline-based anatomical attributes are reported in the Supplementary Material.

To evaluate the relative contribution of the lesion severity and anatomy alone and of the overall anatomical LAD features in predicting MI, a second cohort (LAD_{NL}) was generated from the original one (LAD₀), where the main lesion was artificially removed from each 3D LAD model. The removal of the main lesion was performed using the tool morphMan (Bergersen et al., 2020), which linearly interpolates the cross-sectional area between the proximal and distal edges of the lesion segment.

2.3. Statistical shape modelling

Two different SSMs were built starting from LAD₀ and LAD_{NL} cohorts. Technically, an approach combining Principal Component

Analysis (PCA) with Fisher's linear discriminant analysis (LDA) was adopted, where outputs of PCA were provided as input to LDA. This approach aimed to detect LAD pathological shape features linked to the occurrence of MI.

In this study, following a previously proposed strategy (Aldieri et al., 2024, 2022, 2020), the SSM construction relied on the mathematical framework of the open-source code Deformetrica (Durrleman et al., 2014) (<https://www.deformetrica.org>). Deformetrica allows the computation of a template \bar{T} , representing the average anatomical shape of the population, and of the so-called moment vectors β^i , vessel-specific vectors centered at a common control points grid that define the three-dimensional elastic deformation (Φ^i) the template should undergo to match each i^{th} vessel-specific shape T^i , according to:

$$T^i = \Phi^i \cdot \bar{T} + \varepsilon^i \quad (2)$$

where ε^i is a residual term added to obviate features not captured by the deformation of the template alone. The 3D deformation function Φ^i mapping the template to each vessel-specific shape is represented through the Large Deformation Diffeomorphic Metric Mapping (LDDMM) approach (Durrleman et al., 2014). Technically, Φ^i can be parametrized with a time-varying velocity vector field for each node x of the template surface mesh with an initial velocity vector v_0^i defined as follows:

$$v_0^i(x) = \sum_k K_V(x_k, x) \cdot \beta_{x_k}^i \quad (3)$$

where v_0^i is embedded into a reproducible kernel Hilbert space V with a

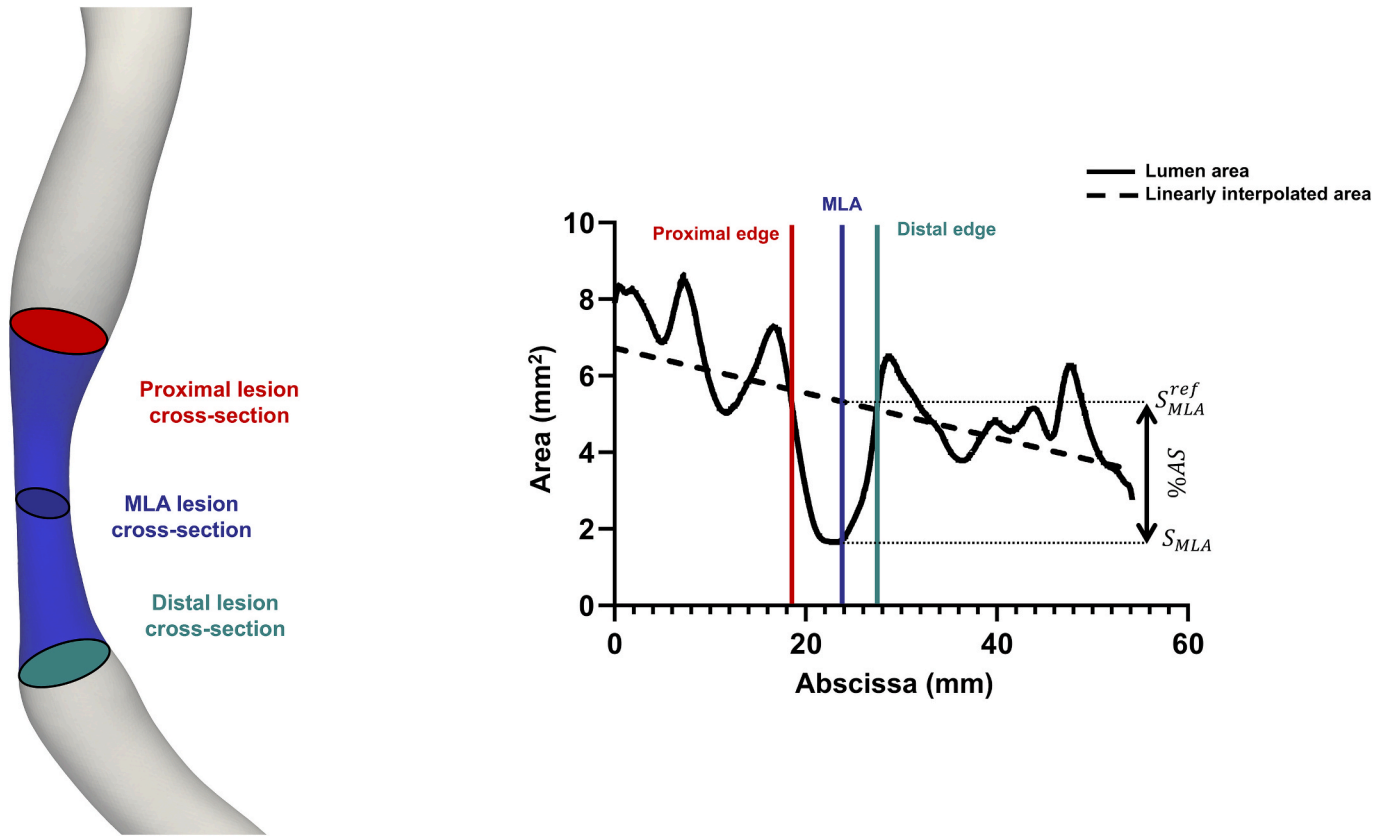


Fig. 2. The lesion segment (LS) visualized on the surface of one LAD model of the cohort under study (left panel) and the anatomical definition of the lesion segment through 3D-QCA (right panel). The trend of the cross-sectional area along the abscissa is shown with the linearly interpolated lumen area (dotted line), with minimum lumen cross-sectional area, distal and proximal edges delimiting the LS indicated.

gaussian kernel K_V of width equal to λ_V , for any pair (x_k, x) , x_k being the location of the control points defined based on the template itself (Durrleman et al., 2014). The moment vectors $\beta_{x_k}^i$ fully define v_0^i , and consequently, the 3D transformation functions $\Phi(\beta^i)$ required for the template to match the shape of each individual vessel in the cohort. Further mathematical details underlying the theoretical framework used in this study can be found in Aldieri et al. (2020), in Durrleman et al. (2014), and in the Supplementary Material.

As all LAD models were randomly oriented in space without a common reference system, they were re-aligned prior to using Deformetrica, as further detailed in the Supplementary Material. Deformetrica was then employed to obtain the template and moment vectors estimation. To identify the optimal user-defined input parameters for the Deformetrica analysis, a sensitivity analysis was conducted. Moreover, after establishing Deformetrica optimal input settings, a 10-fold cross-validation strategy (Bruse et al., 2016) was implemented to identify possible single 3D geometries significantly affecting the template estimation. Exhaustive details on the sensitivity analysis and 10-fold cross-validation are reported in the Supplementary Material.

2.3.1. PCA-based statistical shape model

PCA (Jolliffe and Cadima, 2016) was used to extract the main anatomical variations characterizing the LAD cohort under study. Specifically, the moment vectors obtained from Deformetrica, following the afore-mentioned sensitivity analysis and 10-fold cross validation, were gathered in one single shape matrix \mathbf{X}_β , with each row containing the x, y, z components of the vessel-specific moment vectors. Hence, a $N \times 3k$ shape matrix was obtained as shown in Eq. (4), with N equal to the number of LADs in the cohort and k the number of control points.

$$\mathbf{X}_\beta = \begin{bmatrix} \beta_{x,1}^1 \beta_{y,1}^1 \beta_{z,1}^1 & \dots & \beta_{x,k}^1 \beta_{y,k}^1 \beta_{z,k}^1 \\ \vdots & \ddots & \vdots \\ \beta_{x,1}^N \beta_{y,1}^N \beta_{z,1}^N & \dots & \beta_{x,k}^N \beta_{y,k}^N \beta_{z,k}^N \end{bmatrix} \quad (4)$$

PCA was thus applied onto the shape matrix \mathbf{X}_β , and allowed to retrieve the main shape modes characterizing the analyzed LAD cohort, along with their associated variance, (Aldieri et al., 2020; Cootes et al., 1995; Jolliffe and Cadima, 2016). The corresponding PCA scores p were obtained by projecting the moment vectors matrix \mathbf{X}_β onto the derived PCA modes. These scores thus represent vessel-specific shape features, expressed within the reference system identified by the PCA modes. PCA was performed twice: (i) on the shape matrix coming from Deformetrica run on the LAD₀ cohort; and (ii) on the shape matrix obtained from Deformetrica analysis on the LAD_{NL} cohort. Hence, two distinct PCA scores matrices \mathbf{P} (\mathbf{P}_0 and \mathbf{P}_{NL} , respectively) were obtained, which were employed to perform LDA.

2.3.2. Linear discriminant analysis

LDA (Fisher, 1938) was employed to investigate the capability of the SSM-based shape features to discriminate between lesions culprit for future MI and non-culprit for future MI. While PCA relies on the maximization of shape variance, LDA takes into account the label of the data (*i.e.*, FCL and NCL) by projecting them onto a new space that maximizes class separation (Hermida et al., 2023; Martinez and Kak, 2001; Varela et al., 2017). Hence, here the PCA-LDA combined approach was adopted. More in detail, the PCA scores p_j^i corresponding to the selected PCA modes were gathered into a $N \times m$ matrix \mathbf{P} (Eq. (5)), which was given as input to the LDA algorithm.

$$\mathbf{P} = \begin{bmatrix} p_1^1 & \cdots & p_m^1 \\ \vdots & \ddots & \vdots \\ p_1^N & \cdots & p_m^N \end{bmatrix} \quad (5)$$

By construction, the maximum number of nonzero eigenvectors solving the problem is $c - 1$, with the number of classes $c = 2$ (FCL and NCL) for this specific analysis (Martinez and Kak, 2001). Therefore, one eigenvector was obtained representing the one-dimensional (1D) LDA hyperplane \mathbf{W} together with the related variance σ_{LDA}^2 (Hermida et al., 2023; Varela et al., 2017). Each vessel shape could eventually be represented with a unique score (Z-score) through projection of matrix \mathbf{P} onto the LDA hyperplane. The theoretical background concerning LDA is presented in the Supplementary Material.

LDA was performed considering the PCA scores from both the original LAD₀ cohort and the LAD_{NL} cohort (*i.e.*, \mathbf{P}_0 and \mathbf{P}_{NL}). Specifically, accounting for its ability to maximize classes separation, LDA was carried out three times: (i) on the standardized PCA scores matrix \mathbf{P}_0 , considering the shape features of the LAD₀ cohort; (ii) on the standardized PCA scores matrix \mathbf{P}_{NL} , considering the shape features of the LAD_{NL} cohort; (iii) on the standardized PCA scores matrix \mathbf{P}_{NL} concatenated with the %AS array, thus considering both the shape features of the LAD_{NL} and the information on the severity of the lesion.

Two distinct strategies were adopted to select the PCA scores to be considered for LDA. Firstly, the number of PCA scores able to explain at least 95% of the total variance in the population was selected for each case (LAD₀ and LAD_{NL}) and LDA performed. Secondly, aiming to reduce the risk of overfitting due to an excessive number of features with respect to the dataset dimensionality, a reduced number n of PCA scores was selected to be used as input features for LDA according to the following empirical formulation:

$$n \cdot 3 \cdot c \leq M \quad (6)$$

where c is the number of classes ($c = 2$, NCL and FCL classes) and M is equal to the number of vessels in each class ($M = 33$, the dimensionality of the smallest class, *i.e.*, the NCL class) (Liu and Gillies, 2016). Two different approaches were employed for identifying the reduced subset of n PCA scores from both \mathbf{P}_0 and \mathbf{P}_{NL} : (i) taking into account the first n PCA scores in terms of explained variance and (ii) using a feature selection process based on Kruskal-Wallis statistical test, where a relevance score defined as $-\log(p)$, p being Kruskal-Wallis p-value, was assigned to each PCA score based on its discriminative power in separating FCL and NCL groups (Prabhakar and Lee, 2020). Kruskal-Wallis test was applied within a leave-one-out framework, where the test was repeated over 69 iterations, with one vessel excluded in each iteration. The relevance scores obtained in each iteration were then summed for each PCA score. The n PCA scores with the highest cumulative relevance scores were selected for use in the subsequent LDA.

2.4. Statistical analysis

C-statistics was employed to assess the predictive capability for future MI of %AS and of the identified LDA hyperplanes. Receiving operator characteristics (ROC) curves were analyzed in terms of area under the curve (AUC) and compared using DeLong test (DeLong et al., 1988). Specifically, the discrimination capacity of the LDA-derived anatomical features was evaluated using a leave-one-out cross-validation (LOOCV) (Hermida et al., 2023; Liu et al., 2024; Varela et al., 2017). Mann-Whitney's U test was employed to assess differences in continuous variables between the FCL and NCL groups. A p-value < 0.05 was considered statistically significant for all the statistical analyses, which were conducted with R statistical software, version 4.4.1 (R Foundation for Statistical Computing, Vienna, Austria).

3. Results

3.1. PCA

The optimal combination of Deformetrica inputs yielded a total of 64 moment vectors $\beta(x, y, z)$, with a resulting 69x192 moment vectors matrix \mathbf{X}_β for both cohorts. Outcomes from the sensitivity analysis and the 10-fold cross-validation are provided in the Supplementary Material.

The cumulative variance explained considering a progressively higher number of PCA modes is presented in Fig. 3 for both LAD₀ and LAD_{NL} cohorts. For the original LAD₀ cohort, 16 PCA modes explained at least 95% of total shape variability (Fig. 3, left panel), with the first 3 modes explaining 66% of the total variance (Fig. 4, upper panel). For the artificial LAD_{NL} cohort, a total of 13 PCA shape modes explained at least 95% of total shape variability (Fig. 3, right panel), with the first 3 modes associated with 70% of total variance (Fig. 4, middle panel). For each cohort, all PCA shape modes accounting for 95% of the total shape variance are shown in Fig. S3 of the Supplementary Material. The scores corresponding to the LAD₀ and LAD_{NL} PCA modes were all significantly correlated up to the first 11 modes ($p < 0.02$), the first three PCA modes being strongly correlated ($R > 0.96$, $p < 0.0001$) (Fig. 4, lower panel).

3.2. LDA: Association between SSM-based shape features and future MI

The first 16 PCA scores for LAD₀ and the first 13 PCA scores for LAD_{NL}, explaining 95% of the variance of the population they were extracted from, were employed for the first LDA performance.

The empirically determined optimal number n of PCA scores to be employed for the further LDA, aiming at reducing overfitting, turned out to be five. LOOCV on LDA performed on the first 5 PCA scores in terms of explained variance (accounting for 75% and 79% of the total shape variance in LAD₀ and LAD_{NL} cohorts, respectively) yielded AUC values of 0.56 (95% CI 0.42–0.70, $p > 0.05$) for LAD₀, 0.58 (95% CI 0.44–0.72, $p > 0.05$) for LAD_{NL} and 0.67 (95% CI 0.54–0.80, $p < 0.05$) for LAD_{NL}+%AS, thus demonstrating poor performances in discriminating between FCL and NCL vessels.

The five PCA scores identified based on Kruskal-Wallis statistical test and used for the additional LDA were PCA scores 6, 10, 14, 22, 33 for LAD₀, and PCA scores 9, 19, 25, 35, 55 for LAD_{NL}. These scores were associated to 7.2% and 2.3% of the total shape variance in LAD₀ and LAD_{NL}, respectively. The corresponding PCA modes are displayed in Fig. S4 in the Supplementary Material.

Fig. 5 shows the comparison between the ROC curves resulting from the LOOCV on LDA when the number of PCA scores explained 95% of the total variance and the five highly-ranked PCA scores were used. The selection of these five highly-ranked PCA scores for LDA considerably improved the discrimination performances. In detail, the combination of %AS and LAD_{NL} led to a significantly higher capacity (AUC = 0.97, 95% CI 0.93–1, $p < 0.0001$), compared to %AS alone (AUC = 0.76, 95% CI 0.65–0.87, $p < 0.001$), LAD₀ (AUC = 0.77, 95% CI 0.66–0.89, $p < 0.0001$) and LAD_{NL} (AUC = 0.86, 95% CI 0.78–0.95, $p < 0.0001$) in separating FCL and NCL. No statistically significant differences emerged between LAD₀ and LAD_{NL}.

When the PCA score showing the highest Kruskal-Wallis-based relevance score in each cohort (PCA score 14 for LAD₀ cohort, and PCA score 35 for LAD_{NL} cohort) was considered individually, the LOOCV yielded an AUC value of 0.62 (95% CI 0.48–0.75, $p > 0.05$) for LAD₀ and an AUC value of 0.68 (95% CI 0.55–0.81, $p < 0.01$) for LAD_{NL}. An AUC value equal to 0.84 (95% CI 0.74–0.93, $p < 0.0001$) was obtained for LAD_{NL}+%AS, indicating a good discrimination capacity. Statistically significant differences were found between LAD_{NL}+%AS and LAD₀, LAD_{NL} alone and %AS alone ($p < 0.05$ in all three cases). The corresponding ROC curves are shown in Fig. S6 of the Supplementary Material.

The LDA modes corresponding to the LAD₀, LAD_{NL} and LAD_{NL} with the addition of %AS (LAD_{NL}+%AS) obtained considering the reduced

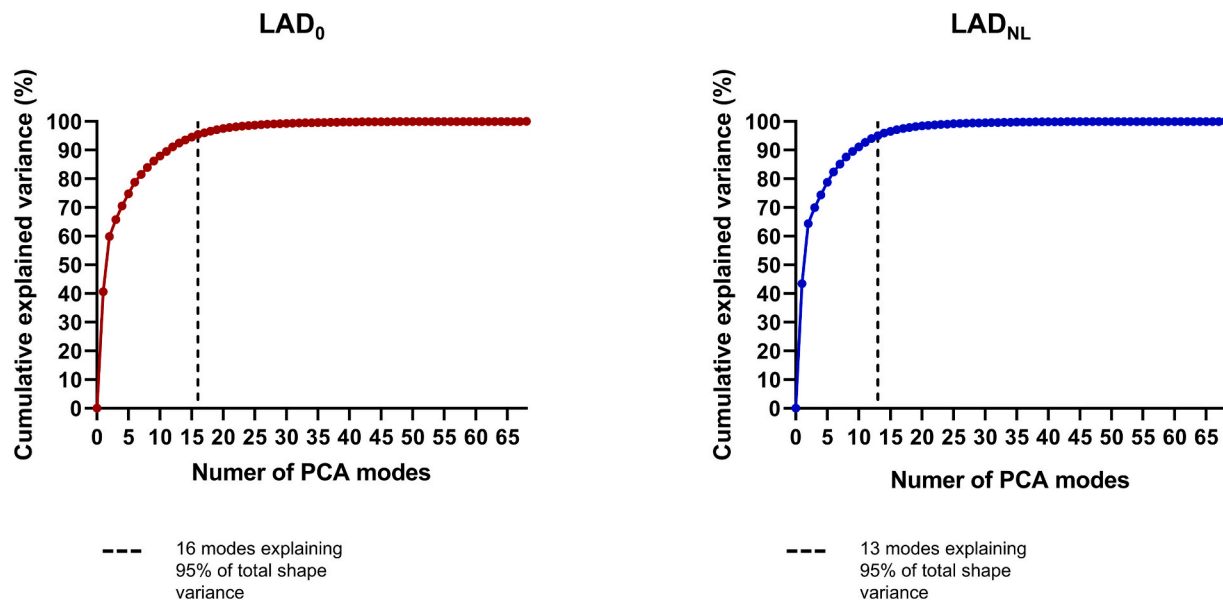


Fig. 3. Cumulative explained variance (%) as a function of the number of PCA modes for the LAD₀ cohort (left panel) and the LAD_{NL} cohort (right panel).

subset of highly-ranked five PCA scores are displayed and compared to the template in Fig. 6 (left panel). The LDA modes present anatomical similarities. As expected, the local narrowing due to the presence of the main lesion is visually identifiable only in the LAD₀-related LDA mode. Fig. 6 (right panel) also shows the comparison of the Z-scores for the three identified LDA modes between FCL and NCL vessels: significant differences ($p < 0.0001$) emerged in the LAD₀, in the LAD_{NL}, and in the LAD_{NL}+%AS cohorts.

The same analysis was conducted on the LDA modes corresponding to the LAD₀, LAD_{NL} and LAD_{NL} with the addition of %AS (LAD_{NL}+%AS) considering all PCA scores explaining 95% of total shape variance and is shown in the Supplementary Material (Fig. S7).

The distributions of %AS, mean curvature, mean torsion, and tortuosity characterizing the LAD₀ cohort, presented in Fig. 7, show that the only significant difference emerged between FCL and NCL vessels was in terms of %AS ($p < 0.0001$).

4. Discussion

Motivated by the intricate interplay between coronary anatomy and hemodynamics in CAD, this study explored the existence of anatomic attributes of LAD coronary arteries, beyond the canonical anatomical lesion severity indicators (Calvert et al., 2011; Stone et al., 2012), that may aid in discriminating future MI.

Although vascular anatomy is known to impact hemodynamic quantities (Bijari et al., 2012; Friedman et al., 1983; Gallo et al., 2015; Lee et al., 2008; Morbiducci et al., 2016), canonical centerline-based anatomical attributes of a coronary vessel have been demonstrated (i) to align only moderately with lesion functional relevance, and (ii) to be improvable in terms of their capacity to discriminate for future adverse events (Candrea et al., 2024; Kashyap et al., 2022; Zhang et al., 2024). In this context, recent studies highlighted the key role played by the luminal narrowing anatomy at the site of the lesion in CAD outcome (Candrea et al., 2022b, 2024) with clinical imaging and in particular 3D-QCA being employed to extract anatomically attributes adopted to support clinical decision-making (Suzuki et al., 2020).

Guided by this emerged centrality of coronary anatomical attributes in the clinical practice, this study expanded the analysis of LAD anatomy to the overall vessel level, testing the hypothesis that anatomical features other than the main lesion could be capable to discriminate lesions culprit of future MI. The proposed anatomy-based analysis employs

statistical shape modelling, a method chosen for its ability to capture comprehensive and independent anatomical features that extend beyond those strictly related to the anatomical lesion severity.

The key outcome of this study is that LDA, especially when performed on selected features commensurate with the limited number of observations, successfully identified anatomical attributes of LAD coronary arteries, apart from area stenosis, with discriminant capability for predicting future MI. This is supported by the finding that, contrarily to torsion, curvature, and tortuosity, significant differences emerged between FCL and NCL vessels in both the LDA₀ and LDA_{NL} cohorts through PCA-LDA analysis. These differences reflect in the fact that the AUC values resulting from the combined PCA-LDA statistical modelling approach turned out to be significant in discriminating lesion culprits of future MI in both the LDA₀ and LDA_{NL} cohorts. Given that canonical centerline-based attributes of the vessel did not exhibit remarkable discrimination capacity for future MI, the findings of the study suggest that key factors other than %AS are hidden in the overall anatomical shape of the vessel, and that such factors have the potential to be used as hallmarks of future MI that can be easily extracted from a 3D-QCA-based analysis. This seems to confirm growing evidence disclosing a strong association between the overall atherosclerotic burden and the risk for adverse coronary events (Arbab-Zadeh and Fuster, 2015; Vergallo et al., 2025). In this study, the addition of %AS to LAD_{NL} caused a significant increase in NCL vs. FCL discrimination capacity with respect to LAD₀, LAD_{NL} and %AS. While LAD₀ cohort inherently reflected the overall atherosclerotic burden of the vessel, by removing the most severe lesion to create the LAD_{NL} cohort we purged the contribution of %AS to the atherosclerotic burden, thus retaining the widespread atherosclerotic narrowing throughout the vessel with the exclusion of the main lesion severity (quantified by %AS). The contribution of the atherosclerotic burden beyond the main lesion severity, inherently difficult to quantify, is thus isolated and considered in the LAD_{NL} cohort. Furthermore, its role is examined in comparison to %AS, which provides quantitative information only about the most severe lesion in the vessel but does not account for its location along the vessel or the presence of other lesions in the same vessel. Our analysis supports the hypothesis that the overall atherosclerotic burden (in terms of combination of widespread atherosclerotic plaque throughout the vessel, and the most severe lesion quantifiable using %AS) leads to future adverse events: taken together, LAD_{NL} and %AS include anatomical information related to the entire atherosclerotic burden.

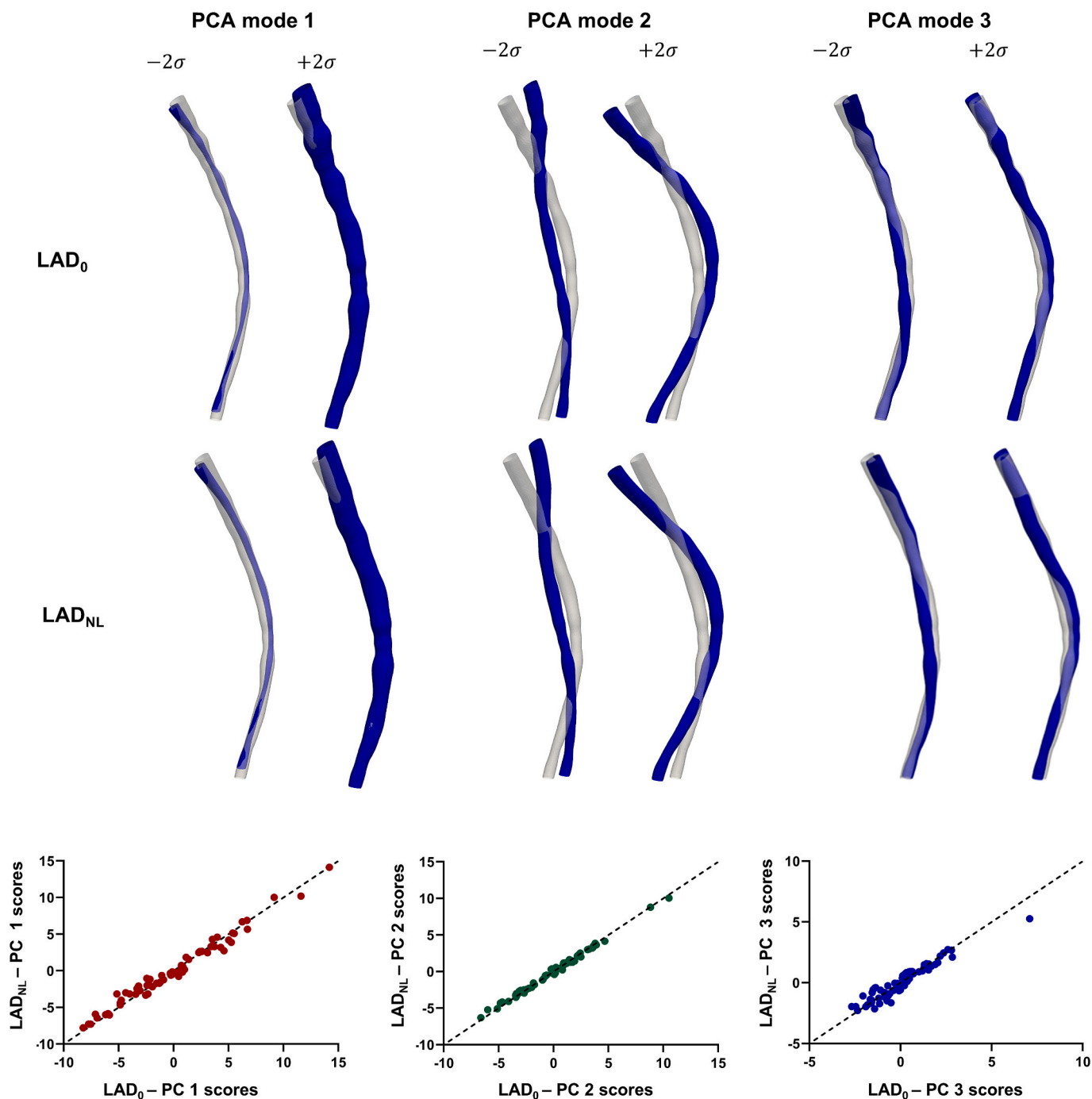


Fig. 4. The first 3 PCA modes (blue) for both the LAD₀ cohort (upper panel) and for the LAD_{NL} cohort (middle panel) are represented by deforming the template (grey) of $\pm 2\sqrt{\sigma^2}$ along each mode, σ^2 representing each specific PCA mode variance. The first 3 modes account for 66% and 70% of total shape variability for the LAD₀ and LAD_{NL} cohorts respectively. In the lower panel the scatter plots of the PCA scores for the original cohort vs. the cohort without main lesion for the first three PCA modes ($R > 0.96$, $p < 0.0001$) are depicted. (For interpretation of the references to colour in this figure legend, the reader is referred to the web version of this article.)

Notably, no significant differences emerged between LAD₀ and LAD_{NL} ROC discrimination capability of future MI. This result can be interpreted considering that although LAD₀ cohort reflects the overall atherosclerotic burden of the vessel and thus contains also information on the main lesions (which were removed from LAD_{NL} cohort), such main lesions occur at completely different locations along individual LAD vessels. This interindividual variability in the location of the main lesions along the LAD limits the SSM-based identified PCA shape features from robustly accounting for it. In other words, the intervariability in the main lesions location negatively impacts on the SSM-based

representation of the vessel. On the contrary %AS, a well-established indicator of CAD severity (Candrea et al., 2024; Stone et al., 2012; Suzuki et al., 2020), only carries information on the most severe luminal obstruction, regardless of its location along the vessel. All these observations distilled into the increased discriminatory capacity of the LAD_{NL} SSM-based representation (accounting for the atherosclerotic burden exclusive of the main lesion severity), when combined with %AS (accounting explicitly for the main lesion severity, but independent of its location along the vessel). Moreover, they explain the lower discrimination capacity of LAD₀ with respect to LAD_{NL}+%AS.

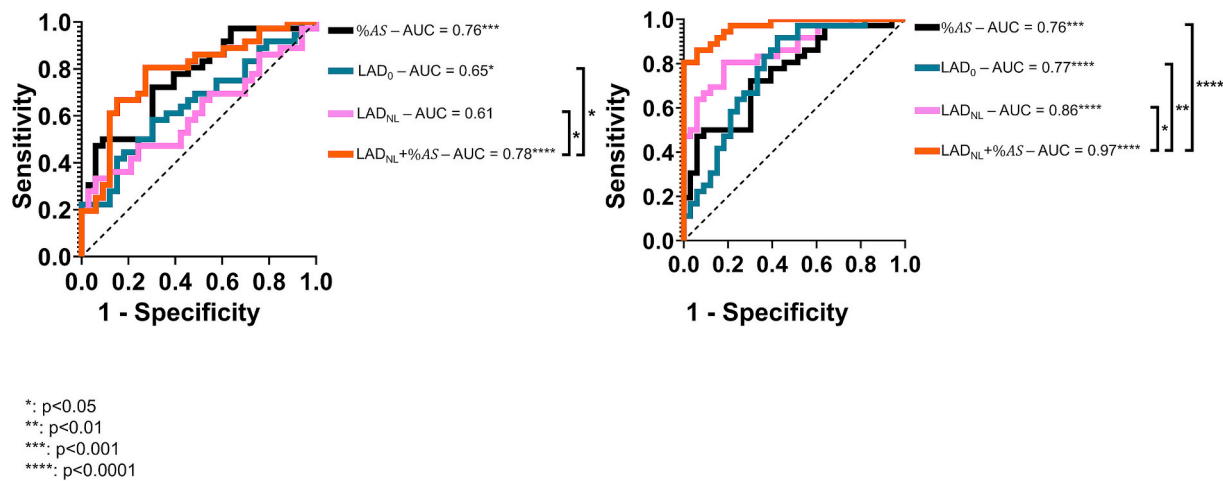


Fig. 5. ROC curves and corresponding AUC values obtained for %AS alone, for the LDA modes associated to the original cohort (LAD_0), to the cohort where for each vessel the most severe lesion has been removed (LAD_{NL}), and to the cohort obtained combining %AS and LAD_{NL} ($LAD_{NL} + \%AS$). ROC curves are shown considering (i) the PCA scores accounting for 95% of the total shape variance (left panel), and (ii) the 5 highly-ranked (*i.e.* the five with the highest discriminatory capability) PCA scores identified based on Kruskal-Wallis test (right panel). The ROC-based analysis refers to LOOCV results.

This study suffers from limitations that could have hampered the generality of its findings. The most impactful limitation of this study lies in the limited number of vessels included, which might have hindered the consistent identification of those anatomical attributes with discriminant capability for future MI, thus complicating the explainability of the model. A further limitation may rely on the wide time range for patients' enrolment, which may limit some of the study's findings related to the MI clinical outcome (Candreva et al., 2022b): as most patients were already receiving treatment at the time of admission, with 76% on aspirin and 90% on statin therapy, an effect of the evolution of medical therapy cannot be excluded *a priori*. However, since the SSM-based approach presented in this study relies solely on anatomical information, the potential bias introduced by pharmacological treatment does not affect its general applicability to other datasets. Additionally, the set of LAD vessels used in this study was derived from a larger dataset presented in a previous work (Candreva et al., 2022b), where vessels were carefully selected based on specific inclusion and exclusion criteria. Notably, patients with bifurcation lesions involving a physiologically significant side branch (*i.e.*, diameter > 2 mm) were excluded. As a result, this study and its findings are focused exclusively on the anatomy of the main segment. However, the proposed SSM-based strategy can be adopted also to populations where lesions at side branches are of clinical interest.

The anatomical interpretation of the identified single LDA modes is not straightforward and more difficult than the interpretation of canonical anatomical attributes: the graphical representation of the LDA modes suggests in fact an association among geometric attributes in the 3D space which is more intricate than the one emerging from the analysis of canonical quantities like curvature or tortuosity, thus highlighting the ability of this approach to detect anatomical features which would otherwise be hard to disclose. Specifically, our analysis showed that the best results in terms of discrimination capacity were obtained when a reduced subset of PCA scores specifically selected based on their ability to discriminate between FCL and NCL classes were considered. These latter correspond to PCA modes that explain only a small portion of the total shape variance, and the canonical anatomical interpretability of PCA modes diminishes as one moves beyond the first few components which account for the majority of shape variance in the population. This outcome suggests that these lesser-variance modes may capture class-specific anatomical features that are not present in the dominant modes, which likely reflect variations common to both classes.

Considering the presented findings, this study paves the way to necessary future investigations that, by including larger datasets, would

allow for testing the robustness of the method on unseen vessel geometries and for identifying new and clinically attainable anatomic attributes with discriminant capacity for future MI.

In conclusion, the findings of this study suggest the existence of anatomical attributes of LAD coronary arteries, beyond the established anatomical lesion severity markers, that significantly discriminate vessels undergoing future MI. Compared to the canonical quantities adopted in the clinical practice to classify the CAD level of a coronary vessel, the anatomical attributes identified through the combined PCA-LDA statistical shape modelling approach performed better in terms of discrimination capacity for future MI also after virtual removal of the main lesion of the vessel, suggesting that not only the main local narrowing of the vessel, but also other LAD anatomical attributes, play a role in CAD outcomes. Furthermore, the discrimination capacity between FCL and NCL was enforced when %AS was added to LDA. Overall, the findings of this study suggest that SSM-based strategies may be helpful to capture the overall atherosclerotic burden of the vessel and eventually to improve the canonical clinical imaging-based decision making performed by interventional cardiologists.

CRediT authorship contribution statement

Bianca Griffo: Writing – review & editing, Writing – original draft, Visualization, Software, Methodology, Investigation, Formal analysis, Data curation, Conceptualization. **Maurizio Lodi Rizzini:** Writing – review & editing, Methodology, Investigation, Formal analysis, Data curation. **Alessandro Candreva:** Writing – review & editing, Investigation, Data curation. **Carlos Collet:** Writing – review & editing, Data curation. **Takuya Mizukami:** Writing – review & editing, Data curation. **Claudio Chiastra:** Writing – review & editing. **Diego Gallo:** Writing – review & editing, Writing – original draft, Supervision, Methodology, Investigation, Formal analysis, Conceptualization. **Umberto Morbiducci:** Writing – review & editing, Writing – original draft, Supervision, Resources, Project administration, Methodology, Investigation, Funding acquisition, Formal analysis, Conceptualization. **Alessandra Aldieri:** Writing – review & editing, Writing – original draft, Visualization, Software, Methodology, Investigation, Formal analysis, Data curation, Conceptualization.

Declaration of competing interest

The authors declare that they have no known competing financial interests or personal relationships that could have appeared to influence

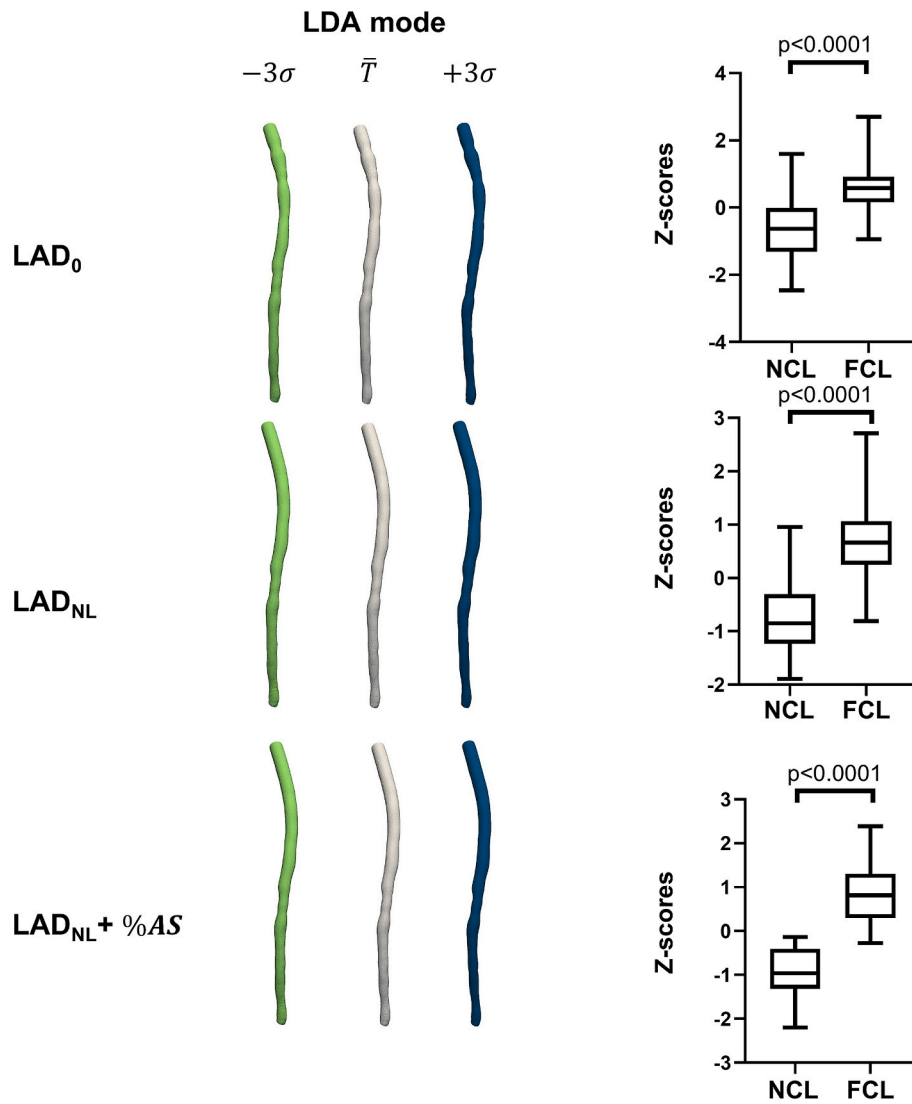


Fig. 6. Left panel: LDA modes corresponding to the original cohort (LAD_0), to the cohort without main stenosis (LAD_{NL}), and to LAD_{NL} with the addition of $\%AS$ ($LAD_{NL} + \%AS$) are represented by deforming the template (grey) along each mode of $\pm 3\sqrt{\sigma^2}$, with σ^2 representing the LDA mode variance. Right panel: box plots depicting the distributions of the Z-scores corresponding to each LDA hyperplane differentiating the original population in NCL and FCL. The results related to LDA hyperplanes built considering PCA scores selected through Kruskal-Wallis statistical test are displayed.

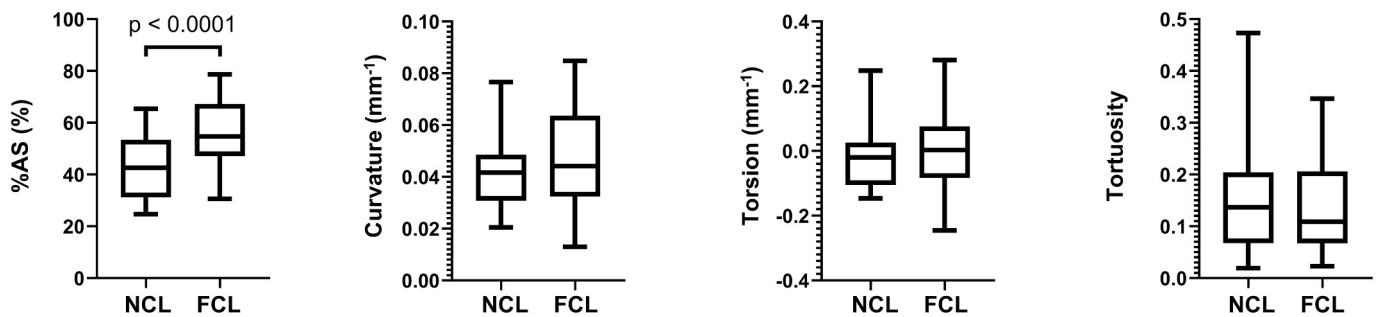


Fig. 7. Box plots depicting the distributions of $\%AS$, mean curvature, mean torsion and tortuosity computed on LAD_0 cohort for FCL and NCL vessels.

the work reported in this paper.

Acknowledgements

This publication is part of the project PNRR-NGEU which has received funding from the MUR – DM 352/2022.

Appendix A. Supplementary data

Supplementary data to this article can be found online at <https://doi.org/10.1016/j.jbiomech.2025.112829>.

Data availability

Data will be made available on request.

References

- Aldieri, A., Bhattacharya, P., Paggiosi, M., Eastell, R., Audenino, A.L., Bignardi, C., Morbiducci, U., Terzini, M., 2022. Improving the Hip Fracture Risk Prediction with a Statistical Shape-and-Intensity Model of the Proximal Femur. *Ann. Biomed. Eng.* 50, 211–221.
- Aldieri, A., Paggiosi, M., Eastell, R., Bignardi, C., Audenino, A.L., Bhattacharya, P., Terzini, M., 2024. DXA-based statistical models of shape and intensity outperform aBMD hip fracture prediction: a retrospective study. *Bone* 182, 117051.
- Aldieri, A., Terzini, M., Audenino, A.L., Bignardi, C., Morbiducci, U., 2020. Combining shape and intensity dxa-based statistical approaches for osteoporotic HIP fracture risk assessment. *Comput. Biol. Med.* 127, 104093.
- Antiga, L., Piccinelli, M., Botti, L., Ene-Iordache, B., Remuzzi, A., Steinman, D.A., 2008. An image-based modeling framework for patient-specific computational hemodynamics. *Med. Biol. Eng. Comput.* 46, 1097.
- Arbab-Zadeh, A., Fuster, V., 2015. The Myth of the “Vulnerable Plaque.”. *J. Am. Coll. Cardiol.* 65, 846–855.
- Asakura, T., Karino, T., 1990. Flow patterns and spatial distribution of atherosclerotic lesions in human coronary arteries. *Circ. Res.* 66, 1045–1066.
- Bentzon, J.F., Otsuka, F., Virmani, R., Falk, E., 2014. Mechanisms of Plaque Formation and Rupture. *Circ. Res.* 114, 1852–1866.
- Bergersen, A.W., Kjeldsberg, H.A., Valen-Sendstad, K., 2020. A framework for automated and objective modification of tubular structures: Application to the internal carotid artery. *Int. J. Numer. Methods Biomed. Eng.* 36, e3330.
- Bijari, P.B., Antiga, L., Gallo, D., Wasserman, B.A., Steinman, D.A., 2012. Improved prediction of disturbed flow via hemodynamically-inspired geometric variables. *J. Biomech.* 45, 1632–1637.
- Bruse, J.L., McLeod, K., Biglino, G., Ntsinjana, H.N., Capelli, C., Hsia, T.-Y., Sermesant, M., Pennec, X., Taylor, A.M., Schievano, S., 2016. A statistical shape modelling framework to extract 3D shape biomarkers from medical imaging data: assessing arch morphology of repaired coarctation of the aorta. *BMC Med. Imaging* 16, 40.
- Calvert, P.A., Obaid, D.R., O’Sullivan, M., Shapiro, L.M., McNab, D., Densem, C.G., Schofield, P.M., Braganza, D., Clarke, S.C., Ray, K.K., West, N.E.J., Bennett, M.R., 2011. Association between IVUS findings and adverse outcomes in patients with coronary artery disease. *J. Am. Coll. Cardiol. Img.* 4, 894–901.
- Candrea, A., De Nisco, G., Lodi Rizzini, M., D’Ascenzo, F., De Ferrari, G.M., Gallo, D., Morbiducci, U., Chiastra, C., 2022a. Current and future applications of computational fluid dynamics in coronary artery disease. *Rev. Cardiovasc. Med.* 23, 377.
- Candrea, A., Lodi Rizzini, M., Calò, K., Pagnoni, M., Munhoz, D., Chiastra, C., Aben, J.-P., Fournier, S., Muller, O., De Bruyne, B., Collet, C., Gallo, D., Morbiducci, U., 2024. Association between automated 3D measurement of coronary luminal narrowing and risk of future myocardial infarction. *J. Cardiovasc. Transl. Res.* 17, 893–900.
- Candrea, A., Pagnoni, M., Rizzini, M.L., Mizukami, T., Gallinoro, E., Mazzi, V., Gallo, D., Meier, D., Shinke, T., Aben, J.-P., Nagumo, S., Sonck, J., Munhoz, D., Fournier, S., Barbato, E., Heggermont, W., Cook, S., Chiastra, C., Morbiducci, U., De Bruyne, B., Muller, O., Collet, C., 2022b. Risk of myocardial infarction based on endothelial shear stress analysis using coronary angiography. *Atherosclerosis* 342, 28–35.
- Collet, C., Amponsah, D.K., Mahendiran, T., Mizukami, T., Wilgenhof, A., Fearon, W.F., 2024. Advancements and future perspectives in coronary angiography-derived fractional flow reserve. *Prog. Cardiovasc. Dis.* 88, 94–104.
- Cootes, T.F., Taylor, C.J., Cooper, D.H., Graham, J., 1995. Active shape models-their training and application. *Comput. Vis. Image Underst.* 61, 38–59.
- Cosentino, F., Raffa, G.M., Gentile, G., Agnese, V., Bellavia, D., Pilato, M., Pasta, S., 2020. Statistical shape analysis of ascending thoracic aortic aneurysm: correlation between shape and biomechanical descriptors. *J. Personalized Med.* 10, 28.
- Cutugno, S., Ingrassia, T., Nigrelli, V., Pasta, S., 2021. On the left ventricular remodeling of patients with stenotic aortic valve: a statistical shape analysis. *Bioengineering* 8, 66.
- De Bruyne, B., Pijls, N.H.J., Kalesan, B., Barbato, E., Tonino, P.A.L., Piroth, Z., Jagic, N., Möbius-Winkler, S., Rioufol, G., Witt, N., Kala, P., McCarthy, P., Engström, T., Oldroyd, K.G., Mavromatis, K., Manoharan, G., Verlee, P., Frobert, O., Curzen, N., Johnson, J.B., Juni, P., Fearon, W.F., 2012. Fractional flow reserve-guided PCI versus medical therapy in stable coronary disease. *N. Engl. J. Med.* 367, 991–1001.
- De Nisco, G., Hartman, E.M.J., Torta, E., Daemen, J., Chiastra, C., Gallo, D., Morbiducci, U., Wentzel, J.J., 2024. Predicting lipid-rich plaque progression in coronary arteries using multimodal imaging and wall shear stress signatures. *Arterioscler. Thromb. Vasc. Biol.* 44, 976–986.
- DeLong, E.R., DeLong, D.M., Clarke-Pearson, D.L., 1988. Comparing the areas under two or more correlated receiver operating characteristic curves: a nonparametric approach. *Biometrics* 44, 837.
- Durrleman, S., Prastawa, M., Charon, N., Korenberg, J.R., Joshi, S., Gerig, G., Trounev, A., 2014. Morphometry of anatomical shape complexes with dense deformations and sparse parameters. *Neuroimage* 101, 35–49.
- Fischer, J.J., Samady, H., McPherson, J.A., Sarembock, L.J., Powers, E.R., Gimple, L.W., Ragosta, M., 2002. Comparison between visual assessment and quantitative angiography versus fractional flow reserve for native coronary narrowings of moderate severity. *Am. J. Cardiol.* 90, 210–215.
- Fisher, R.A., 1938. The statistical utilization of multiple measurements. *Ann. Eugen.* 8, 376–386.
- Friedman, M., Deters, O., Mark, F., Brentbarger, C., Hutchins, G., 1983. Arterial geometry affects hemodynamics: a potential risk factor for atherosclerosis. *Atherosclerosis* 46, 225–231.
- Gallo, D., Steinman, D.A., Morbiducci, U., 2015. An insight into the mechanistic role of the common carotid artery on the hemodynamics at the carotid bifurcation. *Ann. Biomed. Eng.* 43, 68–81.
- Gijsen, F., Katagiri, Y., Barlis, P., Bourantas, C., Collet, C., Coskun, U., Daemen, J., Dijkstra, J., Edelman, E., Evans, P., Van Der Heiden, K., Hose, R., Koo, B.-K., Krams, R., Marsden, A., Migliavacca, F., Onuma, Y., Ooi, A., Poon, E., Samady, H., Stone, P., Takahashi, K., Tang, D., Thondapu, V., Tenekecioglu, E., Timmins, L., Torii, R., Wentzel, J., Serruys, P., 2019. Expert recommendations on the assessment of wall shear stress in human coronary arteries: existing methodologies, technical considerations, and clinical applications. *Eur. Heart J.* 40, 3421–3433.
- Guirav, A., Revaiah, P.C., Tsai, T.-Y., Miyashita, K., Tobe, A., Oshima, A., Sevestre, E., Garg, S., Aben, J.-P., Reiber, J.H.C., Morel, M.A., Lee, C.W., Koo, B.-K., Biscaglia, S., Collet, C., Bourantas, C., Escaned, J., Onuma, Y., Serruys, P.W., 2024. Coronary angiography: a review of the state of the art and the evolution of angiography in cardio therapeutics. *Front. Cardiovasc. Med.* 11, 1468888.
- Haley, H.A., Ghobrial, M., Morris, P.D., Gosling, R., Williams, G., Mills, M.T., Newman, T., Rammohan, V., Pederzani, G., Lawford, P.V., Hose, R., Gunn, J.P., 2021. Virtual (Computed) fractional flow reserve: future role in acute coronary syndromes. *Front. Cardiovasc. Med.* 8, 735008.
- Hermida, U., Stojanovski, D., Raman, B., Ariga, R., Young, A.A., Carapella, V., Carr-White, G., Lukaschuk, E., Piechnik, S.K., Kramer, C.M., Desai, M.Y., Weintraub, W.S., Neubauer, S., Watkins, H., Lamata, P., 2023. Left ventricular anatomy in obstructive hypertrophic cardiomyopathy: beyond basal septal hypertrophy. *Eur. Heart J. – Cardiovasc. Imaging* 24, 807–818.
- Hoogendoorn, A., Kok, A.M., Hartman, E.M.J., De Nisco, G., Casadonte, L., Chiastra, C., Coenen, A., Korteland, S.-A., Van Der Heiden, K., Gijsen, F.J.H., Duncker, D.J., Van Der Steen, A.F.W., Wentzel, J.J., 2020. Multidirectional wall shear stress promotes advanced coronary plaque development: comparing five shear stress metrics. *Cardiovasc. Res.* 116, 1136–1146.
- Jolliffe, I.T., Cadima, J., 2016. Principal component analysis: a review and recent developments. *Philos. Trans. R. Soc. A Math. Phys. Eng. Sci.* 374, 20150202.
- Kashyap, V., Gharleghi, R., Li, D.D., McGrath-Cadell, L., Graham, R.M., Ellis, C., Webster, M., Beier, S., 2022. Accuracy of vascular tortuosity measures using computational modelling. *Sci. Rep.* 12, 865.
- Koo, B.-K., Yang, S., Jung, J.W., Zhang, J., Lee, K., Hwang, D., Lee, K.-S., Doh, J.-H., Nam, C.-W., Kim, T.H., Shin, E.-S., Chun, E.J., Choi, S.-Y., Kim, H.K., Hong, Y.J., Park, H.-J., Kim, S.-Y., Husic, M., Lambrechtsen, J., Jensen, J.M., Nørgaard, B.L., Andreini, D., Maurovich-Horvat, P., Merkely, B., Penicka, M., De Bruyne, B., Ihdaryhid, A., Ko, B., Tzimas, G., Leipsic, J., Sanz, J., Rabbat, M.G., Katchi, F., Shah, M., Tanaka, N., Nakazato, R., Asano, T., Terashima, M., Takashima, H., Amano, T., Sobue, Y., Matsuo, H., Otake, H., Kubo, T., Takahata, M., Akasaka, T., Kido, T., Mochizuki, T., Yokoi, H., Okonogi, T., Kawasaki, T., Nakao, K., Sakamoto, T., Yonetsu, T., Kakuta, T., Yamauchi, Y., Bax, J.J., Shaw, L.J., Stone, P. H., Narula, J., 2024. Artificial intelligence-enabled quantitative coronary plaque and hemodynamic analysis for predicting acute coronary syndrome. *J. Am. Coll. Cardiol. Img.* 17, 1062–1076.
- Kumar, A., Thompson, E.W., Lefieux, A., Molony, D.S., Davis, E.L., Chand, N., Fournier, S., Lee, H.S., Suh, J., Sato, K., Ko, Y.-A., Molloy, D., Chandran, K., Hosseini, H., Gupta, S., Milkas, A., Gogas, B., Chang, H.-J., Min, J.K., Fearon, W.F., Veneziani, A., Giddens, D.P., King, S.B., De Bruyne, B., Samady, H., 2018. High coronary shear stress in patients with coronary artery disease predicts myocardial infarction. *J. Am. Coll. Cardiol.* 72, 1926–1935.
- Lee, J.M., Choi, G., Koo, B.-K., Hwang, D., Park, J., Zhang, J., Kim, K.-J., Tong, Y., Kim, H.J., Grady, L., Doh, J.-H., Nam, C.-W., Shin, E.-S., Cho, Y.-S., Choi, S.-Y., Chun, E.J., Choi, J.-H., Nørgaard, B.L., Christiansen, E.H., Niemen, K., Otake, H., Penicka, M., De Bruyne, B., Kubo, T., Akasaka, T., Narula, J., Douglas, P.S., Taylor, C.A., Kim, H.-S., 2019. Identification of high-risk plaques destined to cause acute coronary syndrome using coronary computed tomographic angiography and computational fluid dynamics. *J. Am. Coll. Cardiol. Img.* 12, 1032–1043.
- Lee, S.-W., Antiga, L., Spence, J.D., Steinman, D.A., 2008. Geometry of the carotid bifurcation predicts its exposure to disturbed flow. *Stroke* 39, 2341–2347.
- Liu, M., Dong, H., Mazlout, A., Wu, Y., Kalyanasundaram, A., Oshinski, J.N., Sun, W., Elefteriades, J.A., Leshnower, B.G., Gleason, R.L., 2024. The role of anatomic shape features in the prognosis of uncomplicated type B aortic dissection initially treated with optimal medical therapy. *Comput. Biol. Med.* 170, 108041.
- Liu, R., Gillies, D.F., 2016. Overfitting in linear feature extraction for classification of high-dimensional image data. *Pattern Recogn.* 53, 73–86.
- Lodi Rizzini, M., Candrea, A., Mazzi, V., Pagnoni, M., Chiastra, C., Aben, J.-P., Fournier, S., Cook, S., Muller, O., De Bruyne, B., Mizukami, T., Collet, C., Gallo, D., Morbiducci, U., 2024. Blood flow energy identifies coronary lesions culprit of future myocardial infarction. *Ann. Biomed. Eng.* 52, 226–238.
- Mansi, T., Voigt, I., Leonardi, B., Pennec, X., Durrleman, S., Sermesant, M., Delingette, H., Taylor, A.M., Boudjemline, Y., Pongiglione, G., Ayache, N., 2011. A Statistical model for quantification and prediction of cardiac remodelling: application to tetralogy of fallot. *IEEE Trans. Med. Imaging* 30, 1605–1616.
- Martinez, A.M., Kak, A.C., 2001. PCA versus LDA. *IEEE Trans. Pattern Anal. Mach. Intell.* 23, 228–233.
- Morbiducci, U., Kok, A.M., Kwak, B.R., Stone, P.H., Steinman, D.A., Wentzel, J.J., 2016. Atherosclerosis at arterial bifurcations: evidence for the role of haemodynamics and geometry. *Thromb. Haemost.* 115, 484–492.

- Munhoz, D., Ikeda, K., Bouisset, F., Sakai, K., Tajima, A., Mizukami, T., Sonck, J., Johnson, N.P., Collet, C., 2024. The role of advanced physiological guidance in contemporary coronary artery disease management. *Curr. Opin. Cardiol.* 39, 520–528.
- Pijls, N.H.J., De Bruyne, B., Peels, K., Van Der Voort, P.H., Bonnier, H.J.R.M., Bartunek, J., Koolen, J.J., 1996. Measurement of fractional flow reserve to assess the functional severity of coronary-artery stenoses. *N. Engl. J. Med.* 334, 1703–1708.
- Prabhakar, S.K., Lee, S.W., 2020. An Integrated Approach for Ovarian Cancer Classification With the Application of Stochastic Optimization. *IEEE Access* 8, 127866–127882.
- Reiber, J.H.C., Van Der Zwet, P.M.J., Koning, G., Von Land, C.D., Van Meurs, B., Gerbrands, J.J., Buis, B., Van Voorthuisen, A.E., 1993. Accuracy and precision of quantitative digital coronary arteriography: Observer-, short-, and medium-term variabilities. *Cathet. Cardiovasc. Diagn.* 28, 187–198.
- Rodero, C., Strocchi, M., Marciniak, M., Longobardi, S., Whitaker, J., O'Neill, M.D., Gillette, K., Augustin, C., Plank, G., Vigmond, E.J., Lamata, P., Niederer, S.A., 2021. Linking statistical shape models and simulated function in the healthy adult human heart. *PLoS Comput. Biol.* 17, e1008851.
- Romero, P., Lozano, M., Dux-Santoy, L., Guala, A., Teixidó-Turà, G., Sebastián, R., García-Fernández, I., 2024. Beyond the root: Geometric characterization for the diagnosis of syndromic heritable thoracic aortic diseases. *Comput. Biol. Med.* 182, 109176.
- Samady, H., Molony, D.S., Coskun, A.U., Varshney, A.S., De Bruyne, B., Stone, P.H., 2020. Risk stratification of coronary plaques using physiologic characteristics by CCTA: Focus on shear stress. *J. Cardiovasc. Comput. Tomogr.* 14, 386–393.
- Sophocleous, F., Bône, A., Shearn, A.I.U., Forte, M.N.V., Bruse, J.L., Caputo, M., Biglino, G., 2022. Feasibility of a longitudinal statistical atlas model to study aortic growth in congenital heart disease. *Comput. Biol. Med.* 144, 105326.
- Steinman, D.A., Migliavacca, F., 2018. Editorial: Special Issue on Verification, Validation, and Uncertainty Quantification of Cardiovascular Models: Towards Effective VVUQ for Translating Cardiovascular Modelling to Clinical Utility. *Cardiovasc. Eng. Technol.* 9, 539–543.
- Stone, G.W., Maehara, A., Lansky, A.J., De Bruyne, B., Cristea, E., Mintz, G.S., Mehran, R., McPherson, J., Farhat, N., Marso, S.P., Parise, H., Templin, B., White, R., Zhang, Z., Serruys, P.W., 2011. A prospective natural-history study of coronary atherosclerosis. *N. Engl. J. Med.* 364, 226–235.
- Stone, P.H., Libby, P., Boden, W.E., 2023. Fundamental pathobiology of coronary atherosclerosis and clinical implications for chronic ischemic heart disease management—the plaque hypothesis: a narrative review. *JAMA Cardiol.* 8, 192.
- Stone, P.H., Maehara, A., Coskun, A.U., Maynard, C.C., Zaromytidou, M., Siasos, G., Andreou, I., Fotiadis, D., Stefanou, K., Papafakis, M., Michalis, L., Lansky, A.J., Mintz, G.S., Serruys, P.W., Feldman, C.L., Stone, G.W., 2018. Role of low endothelial shear stress and plaque characteristics in the prediction of nonculprit major adverse cardiac events. *J. Am. Coll. Cardiol. Img.* 11, 462–471.
- Stone, P.H., Saito, S., Takahashi, S., Makita, Y., Nakamura, S., Kawasaki, T., Takahashi, A., Katsuki, T., Nakamura, S., Namiki, A., Hirohata, A., Matsumura, T., Yamazaki, S., Yokoi, H., Tanaka, S., Otsuji, S., Yoshimachi, F., Honye, J., Harwood, D., Reitman, M., Coskun, A.U., Papafakis, M.I., Feldman, C.L., 2012. Prediction of progression of coronary artery disease and clinical outcomes using vascular profiling of endothelial shear stress and arterial plaque characteristics: the PREDICTION study. *Circulation* 126, 172–181.
- Suzuki, N., Asano, T., Nakazawa, G., Aoki, J., Tanabe, K., Hibi, K., Ikari, Y., Kozuma, K., 2020. Clinical expert consensus document on quantitative coronary angiography from the Japanese Association of Cardiovascular Intervention and Therapeutics. *Cardiovasc. Interv. Ther.* 35, 105–116.
- Swanson, L., Sivera, R., Capelli, C., Alosaimi, A., Mroczek, D., Lam, C.Z., Cook, A., Chaturvedi, R.R., Schievano, S., 2024. A 3D statistical shape model of the right ventricular outflow tract in pulmonary valve replacement patients post-surgical repair. *J. Cardiovasc. Devel. Dis.* 11, 330.
- Thondapu, V., Mamon, C., Poon, E.K.W., Kurihara, O., Kim, H.O., Russo, M., Araki, M., Shinohara, H., Yamamoto, E., Dijkstra, J., Tacey, M., Lee, H., Ooi, A., Barlis, P., Jang, I.-K., 2021. High spatial endothelial shear stress gradient independently predicts site of acute coronary plaque rupture and erosion. *Cardiovasc. Res.* 117, 1974–1985.
- Tufaro, V., Safi, H., Torii, R., Koo, B.-K., Kitslaar, P., Ramasamy, A., Mathur, A., Jones, D. A., Bajaj, R., Erdoğan, E., Lansky, A., Zhang, J., Konstantinou, K., Little, C.D., Rakhit, R., Karamasis, G.V., Baumbach, A., Bourantas, C.V., 2021. Wall shear stress estimated by 3D-QCA can predict cardiovascular events in lesions with borderline negative fractional flow reserve. *Atherosclerosis* 322, 24–30.
- Uren, N.G., Melin, J.A., De Bruyne, B., Wijns, W., Baudhuin, T., Camici, P.G., 1994. Relation between myocardial blood flow and the severity of coronary-artery stenosis. *N. Engl. J. Med.* 330, 1782–1788.
- Varela, M., Bisbal, F., Zacur, E., Berruezo, A., Aslanidi, O.V., Mont, L., Lamata, P., 2017. Novel computational analysis of left atrial anatomy improves prediction of atrial fibrillation recurrence after ablation. *Front. Physiol.* 8, 68.
- Vergallo, R., Park, S.-J., Stone, G.W., Erlinge, D., Porto, I., Waksman, R., Mintz, G.S., D'Ascenzo, F., Seitun, S., Saba, L., Vliegenthart, R., Alfonso, F., Arbab-Zadeh, A., Libby, P., Di Carli, M.F., Muller, J.E., Maurer, G., Gropler, R.J., Chandrashekar, Y. S., Braunwald, E., Fuster, V., Jang, I.-K., 2025. Vulnerable or high-risk plaque. *J. Am. Coll. Cardiol. Img.* 18, 709–740.
- Wentzel, J.J., Chatzizisis, Y.S., Gijsen, F.J.H., Giannoglou, G.D., Feldman, C.L., Stone, P. H., 2012. Endothelial shear stress in the evolution of coronary atherosclerotic plaque and vascular remodelling: current understanding and remaining questions. *Cardiovasc. Res.* 96, 234–243.
- Williams, J.G., Marlevi, D., Bruse, J.L., Nezami, F.R., Moradi, H., Fortunato, R.N., Maiti, S., Billaud, M., Edelman, E.R., Gleason, T.G., 2022. Aortic dissection is determined by specific shape and hemodynamic interactions. *Ann. Biomed. Eng.* 50, 1771–1786.
- Zhang, M., Gharleghe, R., Shen, C., Beier, S., 2024. A new understanding of coronary curvature and haemodynamic impact on the course of plaque onset and progression. *R. Soc. Open Sci.* 11, 241267.